Redox-Associated η^1 to η^2 Conversion of Disulfide Ligands in Dinuclear Ruthenium Complexes

Kumiko Yoshioka, Hayato Kikuchi, Jun Mizutani,† and Kazuko Matsumoto*

Department of Chemistry and Advanced Research Institute for Science and Engineering, Waseda University, Shinjuku-ku, Tokyo 169-8555, Japan, and Japan Science and Technology Corporation, Kawaguchi, Saitama 332-0012, Japan

Received April 14, 2000

Disulfide-bridged dinuclear ruthenium complexes $[\{Ru(MeCN)(P(OMe)_3)_2\}_2(\mu\text{-}X)(\mu,\eta^2\text{-}S_2)][ZnX_3(MeCN)]$ (X = Cl (**2**), Br (**4**)), $[\{Ru(MeCN)(P(OMe)_3)_2\}_2(\mu\text{-}Cl)_2(\mu,\eta^1\text{-}S_2)](CF_3SO_3)$ (**5**), $[\{Ru(MeCN)(P(OMe)_3)_2\}_2(\mu\text{-}Cl)(\mu,\eta^2\text{-}S_2)](BF_4)$ (**6**), and $[\{Ru(MeCN)_2(P(OMe)_3)_2\}_2(\mu\text{-}Cl)(\mu,\eta^1\text{-}S_2)](CF_3SO_3)_3$ (**7**) were synthesized, and the crystal structures of **2** and **4** were determined. Crystal data: **2**, triclinic, $P\bar{1}$, $a = 15.921(4)$ Å, $b = 17.484(4)$ Å, $c = 8.774(2)$ Å, $\alpha = 103.14(2)°$, $\beta = 102.30(2)°$, $\gamma = 109.68(2)°$, $V = 2124(1)$ Å^3, $Z = 2$, R (R_w) = 0.055 (0.074); **4**, triclinic, $P\bar{1}$, $a = 15.943(4)$ Å, $b = 17.703(4)$ Å, $c = 8.883(1)$ Å, $\alpha = 102.96(2)°$, $\beta = 102.02(2)°$, $\gamma = 109.10(2)°$, $V = 2198.4(9)$ Å^3, $Z = 2$, R (R_w) = 0.048 (0.067). Complexes **2** and **4** were obtained by reduction of the disulfide-bridged ruthenium complexes $[\{RuX(P(OMe)_3)_2\}_2(\mu\text{-}X)_2(\mu,\eta^1\text{-}S_2)]$ (X = Cl (**1**), Br (**3**)) with zinc, respectively. Complex **5** was synthesized by oxidation of **2** with $AgCF_3SO_3$. Through these redox steps, the coordination mode of the disulfide ligand was converted from μ,η^1 in **1** and **3** to μ,η^2 in **2** and **4** and further reverted to μ,η^1 in **5**. Electrochemical studies of **6** indicated that similar conversion of the coordination mode occurs also in electrochemical redox reactions.

Introduction

Transition-metal complexes with inorganic sulfide ligands have been widely investigated in relevance to bioinorganic and industrial chemistry.[1] Although most of the reactivities involved in these fields utilize a monosulfide ligand, the disulfide ligand is also noteworthy because of its strong π-donating nature, which remarkably decreases the redox potential of the coordinated metals.[2] It is reported that disulfur ligands bridging two metal atoms have three possible coordination modes: (η^1, η^1), (η^1, η^2), and (η^2, η^2).[3] It is also known that in several examples, conversion of the coordination modes takes place on redox or other reactions of the metals. For example, addition of $F_3C{\equiv}CF_3$ to $(CpV)_2(\mu\text{-}S)_2(\mu{:}\eta^1,\eta^1\text{-}S_2)$ gives $(CpV)_2\{\mu\text{-}(CF_3)_2C_2S_2\}(\mu{:}\eta^2,\eta^2\text{-}S_2)$,[4] and chemical or electrochemical oxidation of $(Cp^*Fe)_2(\mu\text{-}\eta^1,\eta^1\text{-}S_2)(\mu\text{-}\eta^2,\eta^2\text{-}S_2)$ converts the η^1,η^1 ligand into the η^2,η^2 one.[5] In our recent study, reduction of $[\{Ru^{III}Cl(P(OMe)_3)_2\}(\mu\text{-}Cl)_2(\mu,\eta^1\text{-}S_2)]$ (**1**) by sodium metal affords a hexanuclear cluster complex $[Na_2Ru^{II}{}_4(P(OMe)_3)_4(\mu\text{-}Cl)_4(\mu_4\text{-}Cl)_2(\mu,\eta^2\text{-}S_2)_2(\mu\text{-}P(OMe)_3\text{-}P,O)_4]\cdot THF$, in which the coordination mode of the disulfide ligand is converted from μ,η^1 to μ,η^2.[6] In the present study, chemical and electrochemical redox reactions of the disulfide-bridged dinuclear ruthenium complexes were studied in pursuit of a more general view for such redox-associated behavior of disulfide ligands.

Experimental Section

Materials and Methods. Complex $[\{RuCl(P(OMe)_3)_2\}_2(\mu\text{-}Cl)_2(\mu,\eta^1\text{-}S_2)]$ (**1**) was prepared according to the literature.[7] All manipulations were carried out under a nitrogen atmosphere in a drybox (oxygen less than 0.03 ppm (v/v), dew point lower than −60 °C). Dichloromethane, diethyl ether, and acetonitrile of low-water-content grade (water less than 0.003%, 0.005%, and 0.005%, respectively, Kanto Chemical Co., Inc.) were used as purchased without purification. The UV−vis spectra were recorded on a Shimazu UV-3101PC spectrometer, and the NMR spectra were recorded on JEOL EX-270 and JEOL Lambda-270 spectrometers. The ^{31}P chemical shifts were externally referenced to $P(OMe)_3$ in $(CD_3)_2CO$ at 140.0 ppm. The ESR spectrum was recorded on a JEOL RE-2XG spectrometer, and the FAB-MS spectra were recorded on a JEOL JMS-HX110 spectrometer. The cyclic voltammograms were measured by using a BAS CV-50W potentiometer with a Pt working electrode, a Pt wire auxiliary electrode, and an Ag/Ag^+ reference electrode separated from the sample solution via Bu_4NBF_4/MeCN solution. The reference electrode was calibrated to $Fe(C_5H_5)_2/Fe(C_5H_5)_2^+$. The Bu_4NBF_4 used as the supporting electrolyte was recrystallized from ethyl acetate. The molecular orbitals were calculated by using ZINDO in the CaChe software.

* To whom correspondence should be addressed. Address: Department of Chemistry, Waseda University, Shinjuku-ku, Tokyo 169-8555, Japan.
† Current address: School of Science, The University of Tokyo, Bunkyo-ku, Tokyo 113-0033, Japan.

(1) (a) Müller, A.; Diemann, E. *Adv. Inorg. Chem.* **1987**, *31*, 89. (b) Stiefel, E. I.; Chianelli, R. R. In *Nitrogen Fixation: The Chemical−Biochemical−Genetic Interface*; Müller, A., Newton, W. E., Eds.; Plenum Press: New York, 1983; p 341. (c) Rakowskii DuBois, M. *Chem. Rev.*, **1989**, *89*, 1. (d) Newton, W. E. In *Sulfur: Its Significance for Chemistry, for the Geo-, Bio- and Cosmosphere and Technology*; Müller, A., Kreb, B., Eds.; Elsevier: Amsterdam, 1984; p 409. (e) Stiefel, E. I. In *Transition Metal Sulfur Chemistry*; Stiefel, E. I., Matsumoto, K., Eds.; ACS Symposium Series 653; American Chemical Society: Washington, DC, 1996; Chapter 1.
(2) Amarasekera, J.; Rauchfuss, T. B.; Wilson, S. R. *Inorg. Chem.* **1987**, *26*, 3328.
(3) Müller, A.; Jaegermann, W.; Enemark, J. H. *Coord. Chem. Rev.* **1982**, *46*, 245.
(4) Bolinger, C. M.; Rauchfuss, T. B.; Rheingold, A. L. *J. Am. Chem. Soc.* **1983**, *105*, 6321.
(5) (a) Brunner, H.; Merz, A.; Pfauntsch, J.; Serhadli, O.; Wachter, J.; Ziegler, M. L. *Inorg. Chem.* **1988**, *27*, 2055. (b) Inomata, S.; Tobita, H.; Ogino, H. *Inorg. Chem.* **1991**, *30*, 3039.
(6) Matsumoto, K.; Sano, Y. *Inorg. Chem.* **1997**, *36*, 4405.
(7) (a) Matsumoto, T.; Matsumoto, K. *Chem. Lett.* **1992**, 559. (b) Matsumoto, K.; Matsumoto, T.; Kawano, M.; Ohnuki, H.; Shichi, Y.; Nishiide, T.; Sato, T. *J. Am. Chem. Soc.* **1996**, *118*, 2597.

10.1021/ic000392a CCC: $20.00
Published on Web 03/31/2001

[{Ru(MeCN)(P(OMe)$_3$)$_2$}$_2$(μ-Cl)(μ,η^2-S$_2$)][ZnCl$_3$(MeCN)] (2). A suspension of **1** (250 mg, 0.28 mmol) and zinc powder (750 mg, 11.5 mmol) in 10 mL of acetonitrile was stirred at room temperature for 24 h. After removal of the excess zinc by filtration, the filtrate was concentrated to 3 mL under reduced pressure and 7 mL of diethyl ether was added. Yellow crystals of **2** were obtained in 1 d (yield: 204 mg, 65%). Anal. Calcd for $C_{18}H_{45}N_3O_{12}Cl_4P_4S_2ZnRu_2$: C, 19.78; H, 4.15; N, 3.85. Found: C, 19.77; H, 4.41; N, 3.85. ^{1}H NMR (CD_2Cl_2): δ 3.75 (d, $^3J_{P-H}$ = 11.6 Hz), 3.61 (d, $^3J_{P-H}$ = 11.6 Hz), 2.47 (s), 1.98 (s). ^{31}P{^{1}H} NMR (CD_2Cl_2): δ 148.7 (d, $^2J_{P-P}$ = 67.1 Hz), 137.9 (d, $^2J_{P-P}$ = 67.1 Hz). UV−vis (MeCN): λ_{max} 379 nm ($\epsilon = 1.4 \times 10^3$ M^{-1} cm^{-1}). FAB-MS (positive, NBA (=nitrobenzyl alcohol)): *m/e* 880 (M$^+$), 798 (M$^+$ − 2MeCN), 674 (M$^+$ − 2MeCN − P(OMe)$_3$).

[{RuBr(P(OMe)$_3$)$_2$}$_2$(μ-Br)$_2$(μ,η^1-S$_2$)] (3). To a methanol solution (1.0 L) of 4.0 g (15.3 mmol) of RuCl$_3$·3H$_2$O was added 96.3 g of LiBr·H$_2$O (0.92 mol). After the mixture was refluxed for 24 h, PPh$_3$ (24.0 g, 91.5 mmol) was added, and the solution was refluxed for 5 h. The resulting brown solid of RuBr$_2$(PPh$_3$)$_3$ was collected and washed with methanol (yield: 11.4 g, 74% based on RuCl$_3$·3H$_2$O). The solid was dissolved in 1.2 L of hexane, to which 20 mL (169 mmol) of P(OMe)$_3$ was added, and the mixture was refluxed for 2 h. Orange crystals of *trans*-RuBr$_2$(P(OMe)$_3$)$_4$ were obtained by cooling the reaction solution (yield: 5.76 g, 76% based on RuBr$_2$(PPh$_3$)$_3$). The isolated crystals and 0.76 g of elemental sulfur (22.8 mmol) were treated in 200 mL of dichloromethane at room temperature for 24 h. In the course of the reaction, the solution turned from reddish yellow to violet. Condensation of the reaction solution to a half and slow introduction of diethyl ether vapor gave violet needle crystals of **3** (yield: 2.88 g, 70% based on *trans*-RuBr$_2$(P(OMe)$_3$)$_4$). Anal. Calcd for $C_{12}H_{36}O_{12}P_4Br_4S_2Ru_2$: C, 13.32; H, 3.35. Found: C, 13.71; H, 3.44. UV−vis (CH_2Cl_2): λ_{max} 499 nm ($\epsilon = 2.6 \times 10^3$ M^{-1} cm^{-1}), 751 nm ($\epsilon = 7.4 \times 10^3$ M^{-1} cm^{-1}). ^{31}P{^{1}H} NMR(CD_2Cl_2): δ 120.3. The cyclic voltammogram of **3** in MeCN containing 0.1 M Bu_4NBF_4 showed two reversible waves at $E_{1/2}$ = 0.99 and −0.51 V vs Ag/Ag$^+$. Single-crystal X-ray analysis of **3** confirmed that the structure was topologically the same as that of **1** (see the Supporting Information for the structure).

[{Ru(MeCN)(P(OMe)$_3$)$_2$}$_2$(μ-Br)(μ,η^2-S$_2$)][ZnBr$_3$(MeCN)] (4). The compound was prepared in a similar way as for **2** by using **3** instead of **1** (yield: 65%). Anal. Calcd for $C_{18}H_{45}N_3O_{12}Br_4P_4S_2ZnRu_2$: C, 17.01; H, 3.57; N, 3.31. Found: C, 17.11; H, 3.30; N, 3.06. ^{1}H NMR (CD_2Cl_2): δ 3.75 (d, $^3J_{P-H}$ = 11.5 Hz), 3.62 (d, $^3J_{P-H}$ = 11.5 Hz), 2.46 (s), 2.00 (s). ^{31}P{^{1}H} NMR (CD_2Cl_2): δ 149.5 (d, $^2J_{P-P}$ = 63.7 Hz), 136.8 (d, $^2J_{P-P}$ = 63.7 Hz). UV−vis (MeCN): λ_{max} 384 nm ($\epsilon = 1.4 \times 10^3$ M^{-1} cm^{-1}). FAB-MS (positive, NBA): *m/e* 925 (M$^+$), 843 (M$^+$ − 2MeCN), 718 (M$^+$ − 2MeCN − P(OMe)$_3$).

[{Ru(MeCN)(P(OMe)$_3$)$_2$}$_2$(μ-Cl)$_2$(μ,η^1-S$_2$)](CF$_3$SO$_3$) (5). To a dichloromethane solution (10 mL) of **2** (250 mg, 0.23 mmol) was added $AgCF_3SO_3$ (177 mg, 0.69 mmol), and the mixture was stirred at 0 °C for 24 h. The resulting silver metal and AgCl were removed by filtration, and the filtrate was concentrated to 5 mL under reduced pressure. Addition of 7 mL of diethyl ether afforded dark-green crystals of **5** in 1 d (yield: 161 mg, 68%). Anal. Calcd for $C_{17}H_{42}N_2O_{15}F_3Cl_2P_4S_3Ru_2$: C, 19.18; H, 3.98; N, 2.63; S, 9.04; Cl, 6.66. Found: C, 19.03; H, 3.88; N, 2.73; S, 8.97; Cl, 6.39. ESR (MeCN, room temperature): g = 2.050 (X-band, with a symmetrical pair of shoulders at g = 2.039 and 2.061). UV−vis (MeCN): λ_{max} 314 ($\epsilon = 2.6 \times 10^3$ M^{-1} cm^{-1}), 394 ($\epsilon = 1.4 \times 10^3$ M^{-1} cm^{-1}), 432 ($\epsilon = 9.1 \times 10^2$ M^{-1} cm^{-1}), 695 ($\epsilon = 4.2 \times 10^3$ M^{-1} cm^{-1}) nm. FAB-MS (positive, NBA): *m/e* 983 (M$^+$ − 2MeCN + CF_3SO_3), 874 (M$^+$ − MeCN), 834 (M$^+$ − 2MeCN), 800 (M$^+$ − 2MeCN − P(OMe)$_3$), 674 (M$^+$ − 2MeCN − P(OMe)$_3$ − Cl), 585 (M$^+$ − 2MeCN − 2P(OMe)$_3$).

[{Ru(MeCN)(P(OMe)$_3$)$_2$}$_2$(μ-Cl)(μ,η^2-S$_2$)](BF$_4$) (6). Compound **2** (250 mg, 0.23 mmol) and Et_4NBF_4 (50 mg, 0.23 mmol) were treated in 10 mL of dichloromethane for 1 min. After the solution was concentrated under reduced pressure to 4 mL, the resulting white precipitate was removed by filtration. To the filtrate was added 2 mL of dichloromethane, and gradual introduction of diethyl ether vapor into the solution afforded yellow crystals of **6** (yield: 80 mg, 36%). Anal. Calcd for $C_{16}H_{42}N_8BF_4O_{12}ClP_4S_2Ru_2$: C, 19.87; H, 4.38; N, 2.90. Found: C, 20.15; H, 4.44; N, 2.88.

Scheme 1

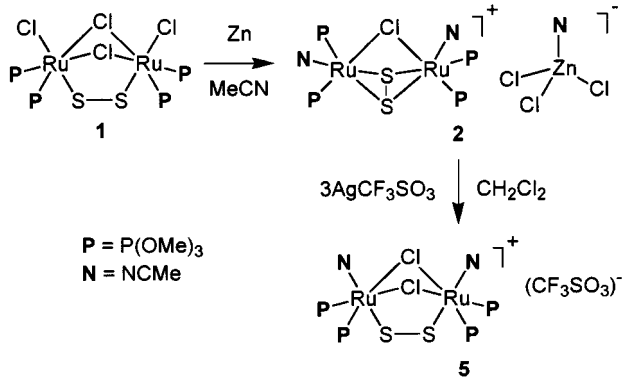

[{Ru(MeCN)$_2$(P(OMe)$_3$)$_2$}$_2$(μ-Cl)(μ,η^1-S$_2$)](CF$_3$SO$_3$)$_3$ (7). To an acetonitrile solution (2 mL) of **1** (90 mg, 0.1 mmol) was added $Me_3SiO_3SCF_3$ (0.1 mL, 0.55 mmol), and the mixture was stirred at room temperature for 3 h. The solution was concentrated to 1 mL under reduced pressure, and 10 mL of diethyl ether was added to give a blue-green powder of **7**, which was washed with diethyl ether three times and was dried under vacuum (yield: 94 mg, 85%). Anal. Calcd for $C_{23}H_{48}N_4F_9O_{21}ClP_4S_5Ru_2$: C, 19.60; H, 3.43; N, 3.98. Found: C, 19.65; H, 3.18; N, 3.67. ^{1}H NMR (CD_3CN): δ 4.02 (d, $^3J_{P-H}$ = 11.2 Hz), 4.00 (d, $^3J_{P-H}$ = 11.2 Hz), 3.67 (d, $^3J_{P-H}$ = 11.2 Hz), 3.65 (d, $^3J_{P-H}$ = 11.2 Hz), 2.73 (s), 2.15 (s). ^{31}P{^{1}H} NMR (CD_3CN): δ 117.6 (d, $^2J_{P-P}$ = 67.8 Hz), 117.2 (d, $^2J_{P-P}$ = 69.8 Hz), 112.9 (d, $^2J_{P-P}$ = 67.8 Hz), 110.6 (d, $^2J_{P-P}$ = 69.8 Hz). UV−vis (MeCN): λ_{max} 412 ($\epsilon = 2.8 \times 10^3$ M^{-1} cm^{-1}), 621 ($\epsilon = 1.3 \times 10^4$ M^{-1} cm^{-1}) nm.

X-ray Structure Determination. Crystals of **2**, **3**, and **4** were attached to thin glass rods and mounted on a Rigaku AFC-7R four-circle diffractometer equipped with a rotating anode X-ray generator (Mo Kα, λ = 0.7107 Å, monochromated with a graphite crystal). The intensity data for **2** and **4** were measured at −50 °C, while those for **3** were measured at −10 °C. Three standard reflections were monitored every 150 reflections, and no decay was observed. An empirical absorption correction based on ψ-scan[8] was applied. The initial phases were obtained by direct methods (SIR92[9] for **2**, and SHELXS86[10] for **3** and **4**), and the structures were refined by using least-squares techniques and difference Fourier syntheses. All the calculations were performed using a teXsan[11] software package. The crystallographic parameters are shown in Table 1.

Results and Discussion

Syntheses and Structures of the η^2 Complexes 2 and 4. Addition of excess amount of zinc powder to the Ru^{III}Ru^{III} complex [{RuCl(P(OMe)$_3$)$_2$}$_2$(μ-Cl)$_2$(μ,η^1-S$_2$)] (**1**) in acetonitrile led to abstraction of the two terminal and one bridging chloride ligands in **1**, giving the Ru^{II}Ru^{II} cation [{Ru(MeCN)(P(OMe)$_3$)$_2$}$_2$-(μ-Cl)(μ,η^2-S$_2$)]$^+$ (the cation of **2**), and the abstracted chloride and zinc ions formed an anion, [ZnCl$_3$(MeCN)]$^-$ (the anion of **2**). During the reaction, the ruthenium was reduced from +3 to +2 (Scheme 1).

The structure of **2** was determined by single-crystal X-ray structure analysis. A drawing of the cation of **2** is shown in Figure 1, and the selected bond distances are listed in Table 2. In the cation, two Ru(MeCN)(P(OMe)$_3$)$_2$ moieties are connected to each other by one chloride and one disulfide bridge. The coordination environment of the ruthenium atoms is virtually

(8) North, A. C. T.; Phillips, D. C.; Mathews, F. S. *Acta Crystallogr., Sect. A* **1968**, *24*, 351.
(9) Altomare, A.; Cascarano, G.; Giacovazzo, C.; Guagliardi, A. *J. Appl. Crystallogr.* **1993**, *26*, 343.
(10) Sheldrick, G. M. *SHELXS86, a program for crystal structure determination*; University of Göttingen: Göttingen, Germany, 1986.
(11) *teXsan, Crystal Structure Analysis Package*; Molecular Structure Corporation: Houston, TX, 1985−1992.

Table 1. Crystallographic Parameters of **2**, **3**, and **4**

	2	**3**	**4**
chemical formula	$C_{18}H_{45}N_3O_{12}Cl_4P_4S_2ZnRu_2$	$C_{12}H_{36}O_{12}Br_4P_4S_2Ru_2$	$C_{18}H_{45}N_3O_{12}Br_4P_4S_2ZnRu_2$
fw	1092.91	1082.19	1270.72
cryst syst	triclinic	triclinic	triclinic
space group	$P\bar{1}$ (No. 2)	$P\bar{1}$ (No. 2)	$P\bar{1}$ (No. 2)
a/Å	15.921(4)	16.888(4)	15.943(4)
b/Å	17.484(4)	23.093(6)	17.703(4)
c/Å	8.774(2)	8.779(2)	8.883(1)
α/deg	103.14(2)	96.52(3)	102.96(2)
β/deg	102.30(2)	101.76(2)	102.02(2)
γ/deg	109.68(2)	90.64(2)	109.10(2)
V/Å^3	2124(1)	3328(1)	2198.4(9)
Z	2	4	2
ρ_{calcd}/g cm^{-3}	1.708	2.160	1.920
μ/cm^{-1}	18.11	60.88	51.54
measd reflns	10 118	15 822	6914
unique reflns	9762	15 299	6611
obsd reflns	7195 ($I > 2.0\ \sigma(I)$)	4113 ($I > 5.0\ \sigma(I)$)	4093 ($I > 1.5\ \sigma(I)$)
no. params	433	645	433
weighting scheme	$w = 1/\sigma^2(F_o) + 0.00034\|F_o\|^2$	$w = 1/\sigma^2(F_o)$	$w = 1/\sigma^2(F_o) + 0.00194\|F_o\|^2$
R^a	0.055	0.041	0.048
$R_w{}^b$	0.074	0.057	0.067
S^c	2.00	1.22	1.14
$\Delta\rho_{max}{}^d$/e$^-$ Å^{-3}	1.03	0.64	0.88
$\Delta/\sigma{}^e$	0.021	0.69	0.002

[a] $R = \sum(|F_o| - |F_c|)/\sum|F_o|$. [b] $R_w = [\sum w(|F_o| - |F_c|)^2/\sum w|F_o|^2]^{1/2}$. [c] $S = \sum w(|F_o| - |F_c|)^2/(N_{obsd} - N_{param})$. [d] Maximum residual electron density in the final difference Fourier map. [e] Maximum shift/error in the final cycle.

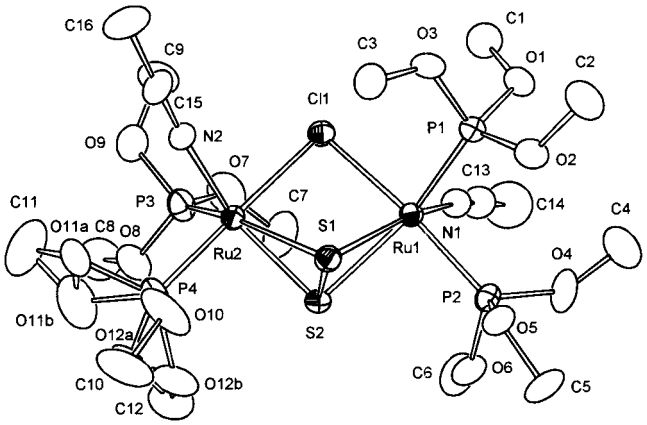

Figure 1. ORTEP drawing of the cation of $[\{Ru(MeCN)(P(OMe)_3)_2\}_2(\mu\text{-}Cl)(\mu,\eta^2\text{-}S_2)][ZnCl_3(MeCN)]$ (**2**) at the 50% probability level.

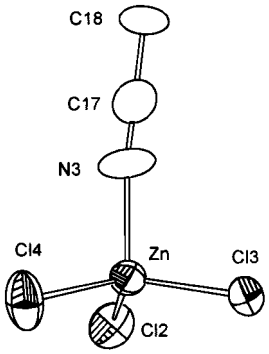

Figure 2. ORTEP drawing of the anion of $[\{Ru(MeCN)(P(OMe)_3)_2\}_2(\mu\text{-}Cl)(\mu,\eta^2\text{-}S_2)][ZnCl_3(MeCN)]$ (**2**) at the 50% probability level.

Table 2. Selected Bond Distances (Å) of **2** and **4**

	2 (X = Cl)	**4** (X = Br)
Ru1−S1	2.348(2)	2.355(3)
Ru1−S2	2.491(2)	2.501(3)
Ru2−S1	2.490(2)	2.490(3)
Ru2−S2	2.345(2)	2.355(3)
Ru1−X1	2.492(2)	2.612(2)
Ru2−X1	2.503(2)	2.623(1)
Ru1−P1	2.215(2)	2.226(3)
Ru1−P2	2.200(2)	2.206(3)
Ru2−P3	2.216(2)	2.229(3)
Ru2−P4	2.218(2)	2.216(3)
Ru1−N1	2.049(6)	2.033(10)
Ru2−N2	2.043(6)	2.03(1)
S1−S2	2.055(3)	2.057(4)
Zn−X2	2.228(3)	2.372(2)
Zn−X3	2.253(3)	2.372(2)
Zn−X4	2.227(3)	2.362(3)
Zn−N3	2.062(8)	2.04(1)

octahedral. The disulfide ligand, which bridged the two ruthenium atoms in a $\mu,\eta^1{:}\eta^1$ mode in the starting complex **1**, is now in the $\mu,\eta^2{:}\eta^2$ coordination mode in **2**. Thus, through the reduction, the disulfide bridge rotates by 90°. The S−S distance in **2** is 2.055(3) Å, which is 0.08 Å longer than that in **1**. The interatomic distance between the two Ru atoms in **2** is ca. 0.13 Å shorter than that in **1**. The structure of the $[ZnCl_3(MeCN)]^-$ anion was determined crystallographically for the first time (Figure 2). The average distance of the Zn−Cl bonds is ca. 2.24 Å, and the distance of the Zn−N bond is 2.062(8) Å. The Zn atom has a virtually tetrahedral coordination environment (the angles around the Zn atom range from 100.8(3)° to 116.3(1)°). The bromide analogue of **2**, $[\{Ru(MeCN)(P(OMe)_3)_2\}_2(\mu\text{-}Br)(\mu,\eta^2\text{-}S_2)][ZnBr_3(MeCN)]$ (**4**), was prepared by using **3** instead of **1**. The structure of **4** is the same as that of **2**. The halogen−metal bond distances in **4** are ca. 0.12 Å longer than the corresponding ones in the chloride complex **2**, while all other distances are not significantly different between the two.

Redox-induced conversion of the coordination mode of a disulfide ligand is reported by Brunner et al.[5a] and Inomata et al.[5b] In their studies, chemical and electrochemical two-electron oxidation of $[Cp^*_2Fe_2(\mu,\eta^1\text{-}S_2)(\mu,\eta^2\text{-}S_2)]$ (Cp^* = 1,2,3,4,5-pentamethylcyclopentadienyl) rotates the $\mu,\eta^1\text{-}S_2$ into $\mu,\eta^2\text{-}S_2$, which is explained in terms of the 18-electron rule; removal of the electrons on oxidation is compensated by the increased hapticity of the disulfide ligand to satisfy the 18-electron rule in both reduced and oxidized forms.[5] In contrast, the present

Scheme 2

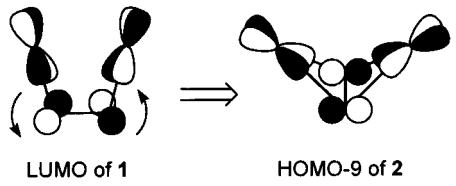

conversion from μ,η^1 to μ,η^2 occurs not on oxidation but on reduction, and the products **2** and **4** do not obey the 18-electron rule. Bolinger et al. reported the conversion of the μ,η^1-S_2 ligand in $(^i\text{PrCp})_2V_2(\mu\text{-S})_2(\mu,\eta^1\text{-S}_2)$ into the μ,η^2 one accompanied by dithiolene ligand formation by addition of hexafluoro-2-butyne to the two μ-S ligands.[12] It is rationalized as follows. Addition of the alkyne-forming dithiolene ligand decreases the electron density on the vanadium atoms, which is compensated by the conversion of the S_2 ligand by use of the higher σ-donating nature of μ,η^1-S_2 compared with that of μ,η^2-S_2. This scheme also seems to be our case because the oxidized $Ru^{III}Ru^{III}$ species has the η^1 form and the reduced $Ru^{II}Ru^{II}$ one has the η^2 form. As another explanation of the conversion, we carried out qualitative molecular orbital calculations of **1** and **2** (Scheme 2). The LUMO of **1** has a Ru−S π-antibonding nature. Thus, the reduction of **1** destabilizes the Ru−S−S−Ru geometry. However, the reduced complex will be stabilized if the disulfide ligand rotates by 90° because in this orientation the signs of the atomic orbitals on the ruthenium and sulfur atoms fit with each other and the molecular orbital will be bonding. Actually, in the calculations of **2** having the η^2-disulfide ligand, the HOMO-9 corresponds to a σ-bonding interaction between the ruthenium and the sulfur atoms. Thus, it is reasonable that addition of electrons to the antibonding LUMO in **1** promotes the conversion from η^1 to η^2, leading to the formation of **2**.

Synthesis of the η^1 Complex 5. Reaction of 3 equiv of $AgCF_3SO_3$ with **2** led to the transfer of one of the chloride ligands in $[ZnCl_3(MeCN)]^-$ to the bridging position between the two ruthenium atoms, together with one-electron oxidation, to give the $Ru^{II}Ru^{III}$ complex $[\{Ru(MeCN)(P(OMe)_3)_2\}_2(\mu\text{-Cl})_2(\mu,\eta^1\text{-S}_2)](CF_3SO_3)$ (**5**) (Scheme 1). We have previously synthesized **5** by the reaction of $[\{RuCl(P(OMe)_3)_2\}_2(\mu\text{-Cl})_2(\mu,\eta^1\text{-S}_2)]$ with sodium metal, and the η^1 nature of the disulfide ligand has been confirmed crystallographically.[13] Thus, in the present reaction, one-electron oxidation of the η^2 complex **2** led to the conversion of the coordination mode of the disulfide ligand into η^1 again.

Electrochemical Behavior of the η^2 Complex. Conversion of the disulfide coordination mode was examined with cyclic voltammetry to see whether the disulfide ligand behaves similarly to the chemical redox reactions. To avoid any possible complexity of the electrochemical reaction expected for $[ZnCl_3(MeCN)]^-$ in **2**, the anion was substituted by BF_4^- and $[\{Ru(MeCN)(P(OMe)_3)_2\}_2(\mu\text{-Cl})(\mu,\eta^2\text{-S}_2)](BF_4)$ (**6**) was used for the following measurement.

The cyclic voltammogram of **6** measured in MeCN at a sweep rate of 50 mV/s is shown in Figure 3. In the first anodic sweep, an oxidation wave (a + b) was observed at 0.07 V (all the potentials are referenced to $Fe(C_5H_5)_2/Fe(C_5H_5)_2^+$), whereas in the following cathodic sweep, two smaller reduction waves appeared at 0.01 V (e) and −0.69 V (g). When the sweep rate was increased to 0.5 V/s (Figure 4), another oxidation peak c

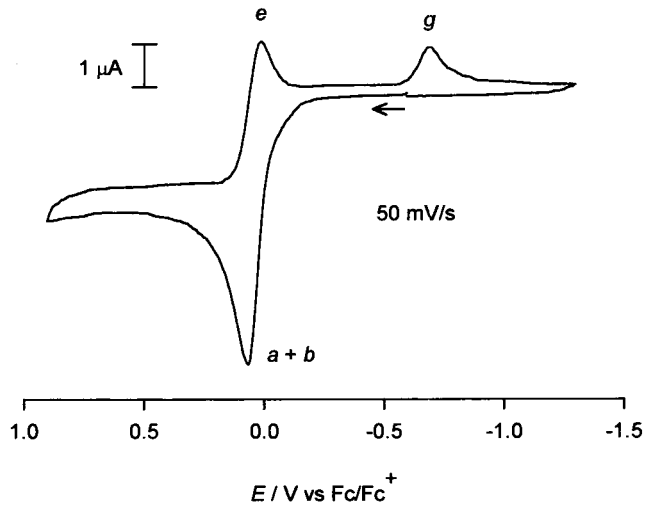

Figure 3. Cyclic voltammograms of $[\{Ru(MeCN)(P(OMe)_3)_2\}_2(\mu\text{-Cl})(\mu,\eta^2\text{-S}_2)](BF_4)$ (**6**) at sweep rate of 50 mV/s.

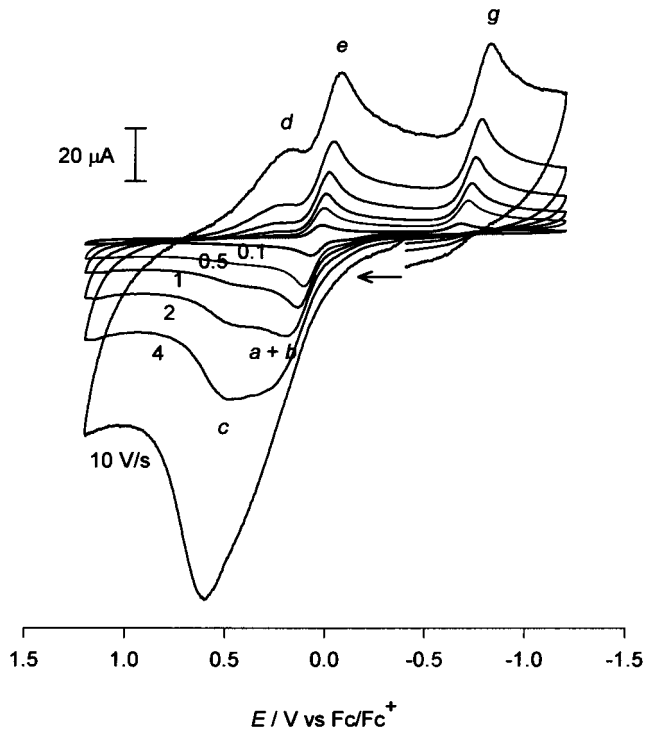

Figure 4. Cyclic voltammograms of $[\{Ru(MeCN)(P(OMe)_3)_2\}_2(\mu\text{-Cl})(\mu,\eta^2\text{-S}_2)](BF_4)$ (**6**) at sweep rate from 0.1 to 10 V/s.

appeared at ca. 0.5 V, which then grew and shifted to ca. 0.6 V on further increase of the sweep rate with a concomitant decrease of the wave a + b. Contrary to this change of the oxidation wave, the reduction waves stayed almost unchanged. On further increase of the sweep rate, i.e., at or above 4 V/s, another reduction wave (d) grew at ca. 0.2 V. These facts suggest that although several different oxidation processes proceed at the increased sweep rate, the final oxidation product is always the same because the reduction waves remain almost unchanged at any sweep rate. When the sweep rate was decreased from 50 to 5 mV/s (Figure 5), the reduction wave g at −0.69 V gradually disappeared and a new small wave f grew at ca. −0.25 V. At the same time, the oxidation wave a + b was gradually separated into two waves, a and b.

The above voltammograms suggest the following electrochemical behavior of **6** (Scheme 3). At sweep rates lower than

(12) Bolinger, C. M.; Rauchfuss, T. B.; Rheingold, A. L. *J. Am. Chem. Soc.* **1983**, *105*, 6321.
(13) Sano, Y. Master Thesis, Waseda University, Tokyo, Japan, 1995.

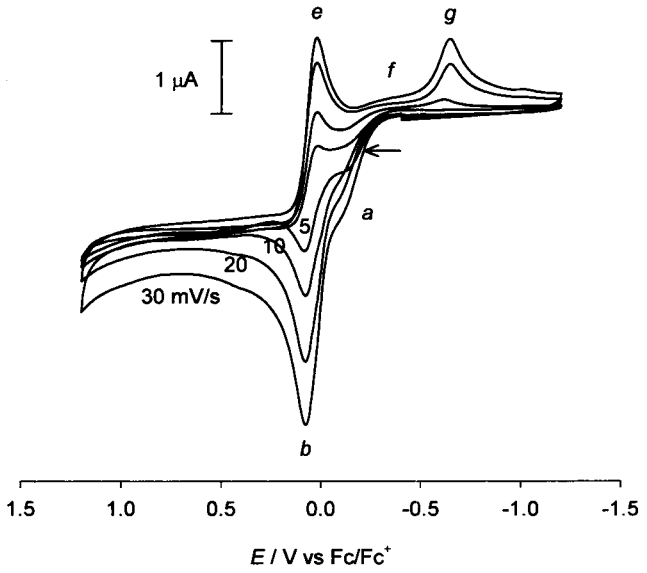

Figure 5. Cyclic voltammograms of $[\{Ru(MeCN)(P(OMe)_3)_2\}_2(\mu\text{-Cl})(\mu,\eta^2\text{-}S_2)](BF_4)$ (**6**) at sweep rate from 5 to 30 mV/s.

Scheme 3

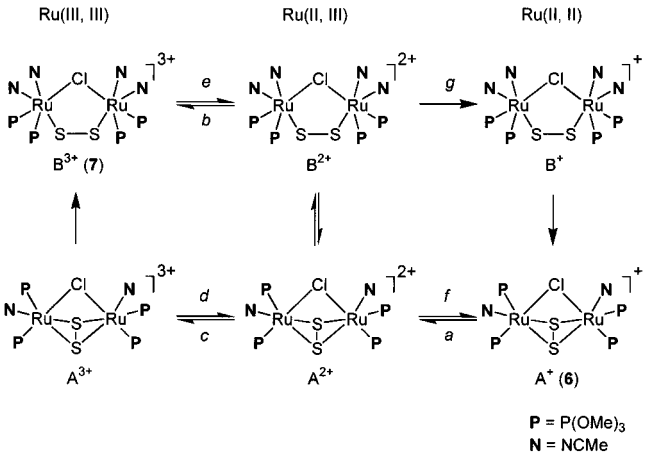

1 V/s, A^+ is one-electron-oxidized to A^{2+} (process a), which is followed by the rearrangement of the disulfide ligand from η^2 to η^1, giving B^{2+}. The species B^{2+} is further oxidized to B^{3+} (process b) at almost the same potential as that of process a. This process from A^+ to B^{3+} is an ECE process.[14] At higher sweep rates, oxidation of A^+ to A^{3+} becomes conspicuous via processes a and c, and A^{3+} thus formed undergoes disulfide rearrangement to give B^{3+}. While this process is dominant at higher sweep rates, the same process (wave c) is still observed as a minor path even at a sweep rate as low as 30 mV/s. Since the sweep rate is so high, process c takes place before the rearrangement from A^{2+} to B^{2+} occurs.

In the cathodic sweep, the reduction wave e at ca. 0.0 V corresponds to the reduction of B^{3+} to B^{2+} (process e), and the reduction wave g at ca. -0.7 V is the reduction of B^{2+} to B^+ (process g). Conversion of the disulfide ligand in B^+ from η^1 to η^2 recovers the starting species A^+. On increase of the sweep rate, a broad wave d appears at ca. 0.2 V, which corresponds to the reduction of A^{3+} to A^{2+}. This wave at ca. 0.2 V appears because at these high sweep rates, conversion of A^{3+} to B^{3+} does not proceed completely and reduction of A^{3+} takes place in parallel. At sweep rate of 10 V/s, the oxidation proceeds via two routes, $A^+ \rightarrow A^{2+} \rightarrow B^{2+} \rightarrow B^{3+}$ and $A^+ \rightarrow A^{2+} \rightarrow A^{3+}$. In the latter route, a portion of the final product A^{3+} is rapidly converted to B^{3+}, and therefore, the reverse cathodic sweep starts with the mixture of A^{3+} and B^{3+}. The reduction of A^{3+} is via either $A^{3+} \rightarrow A^{2+} \rightarrow A^+$ or $A^{3+} \rightarrow A^{2+} \rightarrow B^{2+} \rightarrow B^+ \rightarrow A^+$, and the reduction of B^{3+} is via $B^{3+} \rightarrow B^{2+} \rightarrow B^+ \rightarrow A^+$. The fact that the wave g is slightly larger than e at a sweep rate of 10 V/s indicates that the two reduction routes $A^{3+} \rightarrow A^{2+} \rightarrow B^{2+}$ and $B^{3+} \rightarrow B^{2+}$ merge at the process g.

Scheme 4

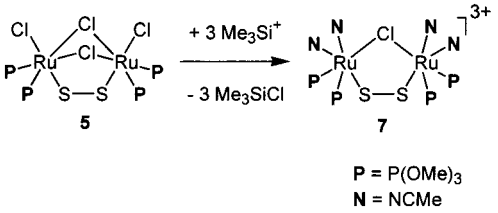

At sweep rates lower than 50 mV/s (Figure 5), waves a and b correspond to processes a and b in Scheme 3, respectively, and the broad cathodic wave at f corresponds to the reverse reaction of process a, i.e., $A^{2+} \rightarrow A^+$. This shows that at very slow sweep rates, rearrangement of B^{2+} to A^{2+} can proceed to some extent, and therefore, the reduction routes $B^{3+} \rightarrow B^{2+} \rightarrow A^{2+} \rightarrow A^+$ and $B^{3+} \rightarrow B^{2+} \rightarrow B^+ \rightarrow A^+$ proceed in parallel. The fact that wave g decreases as wave f becomes more discernible supports the above assignment.

Apparently, the conversion between A^{2+} and B^{2+} is reversible and the conversion rate from A^{2+} to B^{2+} is rapid, while the reverse reaction is very slow. At medium to rapid sweep rates, B^{2+} is further reduced to B^+ before B^{2+} isomerizes to A^{2+}. This is the reason for the disappearance of wave g at very low sweep rates.

Since no direct evidence is yet obtained for the structures of the intermediates A^{2+} and B^{2+}, it is also possible that either or both of these intermediates have the disulfide ligand in the unsymmetric η^1,η^2 mode. But this is less possible because the redox steps a−g are apparently much more rapid than the isomerization processes, and therefore, it is more probable to assign the structures of A^{2+} and B^{2+} as those in Scheme 3.

To confirm the existence of B^{3+} in the electrochemical process, $B^{3+}(CF_3SO_3)^-{}_3$ (**7**) was chemically prepared by removal of three chlorides from **1** by using $Me_3SiO_3SCF_3$ (Scheme 4), and cyclic voltammetry measurements were taken. The voltammogram of **7** was almost the same with that of **6**, which supports the above electrochemical scheme. To further confirm the process in Scheme 3, bulk electrolysis of **6** was carried out at 0.5 V. Although it had been expected that 2 F/mol would be consumed in the bulk electrolysis, less than 1 F/mol was consumed even after 3 h. The ESR spectrum ($g = 2.05$) and the UV−vis spectrum ($\lambda_{max} = 703$ nm) of the resulting solution suggested that $[\{Ru(MeCN)(P(OMe)_3)_2\}(\mu\text{-Cl})_2(\mu,\eta^1\text{-}S_2)]^+$ (**5**) is formed instead of the expected species B^{3+} in solution. This observation can be rationalized as follows (Scheme 5). After the formation of a small amount of B^{3+} ($Ru^{III}Ru^{III}$) by the electrolysis, B^{3+} reacts with remaining **6** ($A^+(BF_4)^-$, $Ru^{II}Ru^{II}$), giving the previously reported complexes $[\{Ru(MeCN)(P(OMe)_3)_2\}(\mu\text{-Cl})_2(\mu,\eta^1\text{-}S_2)]^+$ (**5**, $Ru^{II}Ru^{III}$) and $[\{Ru(MeCN)_3(P(OMe)_3)_2\}(\mu,\eta^1\text{-}S_2)]^{3+}$ (**8**, $Ru^{II}Ru^{III}$).[7b] The cyclic voltammogram of a 1:1 mixture solution of **6** ($A^+(BF_4)^-$) and **7** ($B^{3+}(CF_3SO_3)^-{}_3$) was similar to that of the bulk electrolysis solution. Because there was no indication of the existence of **5**

(14) (a) Heinze, J. *Angew. Chem., Int. Ed. Engl.* **1984**, *23*, 831. (b) Bard, A. J.; Faulkner, L. R. *Electrochemical Methods: Fundamentals and Applications*; Wiley: New York, 1980; Chapter 11.

Scheme 5

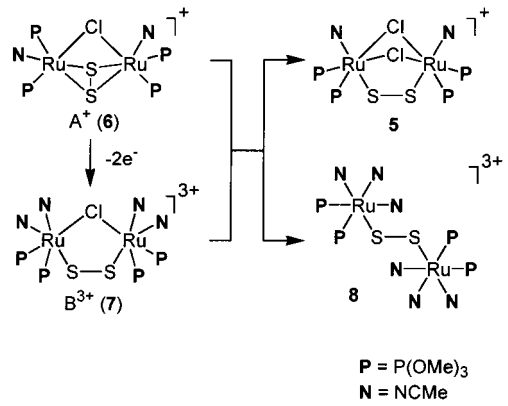

or **8** in the cyclic voltammogram of **6** (vide supra), the above reaction between **6** and **7** must be slow compared to the potential sweep rates.

The whole electrochemical behavior indicates that the Ru^{II}-Ru^{II} species (A^{+}) prefers the η^2 structure and that the $Ru^{III}Ru^{III}$ species (B^{3+}) prefers the η^1 one. For the $Ru^{II}Ru^{III}$ species, A^{2+} and B^{2+} convert to each other, and there is an equilibrium between them. This tendency in the coordination mode of the disulfide ligand is in accordance with the results of the chemical redox reactions in which the $Ru^{II}Ru^{II}$ species prefers the η^2 mode and the $Ru^{III}Ru^{III}$ species the η^1 one.

Acknowledgment. We are grateful to the financial support by CREST (Core Research for Evolutional Science and Technology) of the Japan Science and Technology Corporation.

Supporting Information Available: An X-ray crystallographic file for the structure determination of **3** and X-ray crystallographic files in CIF format for the structure determinations of **2** and **4**. This material is available free of charge via the Internet at http://pubs.acs.org.

IC000392A